

Grain boundary motion in layered phases

Denis Boyer and Jorge Viñals

*School of Computational Science and Information Technology,
Florida State University, Tallahassee, Florida 32306-4120.*

(November 11, 2018)

We study the motion of a grain boundary that separates two sets of mutually perpendicular rolls in Rayleigh-Bénard convection above onset. The problem is treated either analytically from the corresponding amplitude equations, or numerically by solving the Swift-Hohenberg equation. We find that if the rolls are curved by a slow transversal modulation, a net translation of the boundary follows. We show analytically that although this motion is a nonlinear effect, it occurs in a time scale much shorter than that of the linear relaxation of the curved rolls. The total distance traveled by the boundary scales as $\epsilon^{-1/2}$, where ϵ is the reduced Rayleigh number. We obtain analytical expressions for the relaxation rate of the modulation and for the time dependent traveling velocity of the boundary, and especially their dependence on wavenumber. The results agree well with direct numerical solutions of the Swift-Hohenberg equation. We finally discuss the implications of our results on the coarsening rate of an ensemble of differently oriented domains in which grain boundary motion through curved rolls is the dominant coarsening mechanism.

05.45.-a, 47.20.Bp

I. INTRODUCTION

This paper addresses the motion of a grain boundary separating two regions of parallel convective rolls, as can be observed in a Rayleigh-Bénard convection cell of large aspect ratio. Each semi-infinite region (or grain) is comprised of roll patterns of same wavenumber q_0 , but the corresponding wavevectors are mutually perpendicular. Our main focus in this paper is the relationship between local roll curvature and grain boundary motion. Although the model equations used in our analysis are appropriate for Rayleigh-Bénard convection near onset [1], we expect that the qualitative features of our findings also hold in others systems that exhibit layered phases, such as, for example, lamellar phases in weakly segregated block copolymers [2,3].

Consider a disordered system brought into a layered phase, *e.g.* by a temperature quench in the case of a diblock copolymer, or by a change in Rayleigh number in a Rayleigh-Bénard convection cell. Domains comprised of rolls (in Rayleigh-Bénard convection) or lamellae (in block copolymers near a symmetric mixture) quickly form that have a well defined characteristic wavenumber q_0 (in the case of Rayleigh-Bénard convection near threshold, for example, q_0 lies on the marginal stability boundary against a zig-zag instability [4,5]). Due to translational and rotational invariance, the spontaneous relaxation from the initial disordered state leads in practice to a large number of such domains, and a sufficiently large system remains isotropic macroscopically. Such a configuration also contains a large density of defects, such as grain boundaries, disclination and dislocations.

Defect motion in two dimensional layered phases has been studied extensively, especially in connection with the evolution of convective rolls in Rayleigh-Bénard cells [6,7]. A primary question is how defect velocities are related to features of the background surrounding them, such as roll periodicity. It is well known, for example, that dislocations climb [8], or that grain boundary motion between two domains with straight rolls provides a wavelength selection mechanism [9,10]. On the other hand, less attention has been paid to the relationship between defect motion and roll curvature [11]. We study in this paper a particular situation that appears to be prevalent (even if idealized) during the formation and evolution of layered structures: curvature induced motion of a grain boundary separating two semi-infinite ordered domains. We first show that if the rolls of one of the domains are periodically modulated along their transverse direction, the perturbation decays in time with a rate proportional to q^4 , where q is the wavenumber of the modulation. In addition, a novel feature is associated with this relaxation: the average position of the boundary does not remain stationary, but undergoes a net displacement such that the size of the region with straight unperturbed rolls increases. Analytic calculations based on the amplitude equation formalism show that this motion is a nonlinear effect, that it occurs in a time scale much shorter than the linear relaxation of the curved rolls. The total distance traveled by the boundary scales as $\epsilon^{-1/2}$, where ϵ is the reduced Rayleigh number. Consequently, the grain boundary can travel large distances, even for very small initial perturbations.

The analysis of grain boundary motion and relaxation, while interesting in its own right, is also expected to contribute to our understanding of the coarsening of an ensemble of grains. Linear analyses of boundary or defect

motion have already been used in the past to predict coarsening exponents [12,13]. The method reproduces known exponents in the case of models *A* and *B* in the lexicon of Hohenberg and Halperin [14], and has also been used to predict coarsening exponents for $O(N)$ vector models [13] (see also [15,16]). Coarsening laws for layered phases, on the other hand, remain largely unexplained [17,12,5,18–20].

In Section II, we describe the configuration of the grain boundary studied, as well as the model equations. Section III presents a linear stability analysis of long wavelength transverse modulations near the boundary. The numerical method used to validate our solutions is outlined in Section IV, as well as the motivation for the nonlinear analysis given in Section V. Finally, in Section VI, we present conclusions, and briefly discuss possible implications of our results on coarsening rates.

II. GRAIN BOUNDARY CONFIGURATION AND GOVERNING EQUATIONS

The base or reference state is a stationary and planar grain boundary separating two semi-infinite domains *A* and *B* of straight convective rolls. Both sets of rolls have the same wavelength $\lambda_0 = 2\pi/q_0$. It is in general expected from previous studies that such grain boundaries are stable against low wavenumber perturbations [21]. We wish to study here the decay of a perturbation of wavenumber $q \ll q_0$ applied in the direction transverse to the rolls of one of the domains, referred to as to domain *A* (see Fig. 1a). In this article, we consider for all our analytic calculations the particular case in which the two sets of rolls are oriented at right angles relative to each other in the way depicted on Fig. 1b. In this case, the rolls of domain *A* are parallel to the grain boundary itself. We expect that a 90° grain boundary is the boundary of lowest energy, and hence that it is the most common in an extended system that evolves spontaneously. However, our analysis can be generalized to cases such as shown on Fig. 1a, in which *A* and *B* rolls have arbitrary angles with respect to the grain boundary, and we do not anticipate qualitative changes in our conclusions.

Our focus is on transverse modulations since this is the simplest kind of perturbation that induces roll curvature without any average roll compression (compression is associated with longitudinal perturbations along the roll normal). Our study differs from that of ref. [21] in which a grain boundary was perturbed with a modulation of wave vector having components both transverse and longitudinal to the rolls. As was shown in ref. [21], the longitudinal component of the perturbation dominated the relaxation. We analyze here the relaxation of a pure transverse (or curvature) mode, and obtain results that are qualitatively different from those of ref. [21].

Let an order parameter ψ represent, for example, the vertical velocity in the mid-plane of a convecting fluid layer. Just above onset, when the reduced Rayleigh number $\epsilon = (R - R_c)/R_c \ll 1$ (R_c is the critical Rayleigh number for instability), ψ can be expanded as the superposition of two waves with slowly varying complex amplitudes *A* and *B* [1],

$$\psi(x, y, t) = \frac{1}{2} [A(x, y, t) e^{iq_0x} + B(x, y, t) e^{iq_0y} + c.c.]; \quad A|_{x=-\infty} = 0, \quad B|_{x=+\infty} = 0. \quad (2.1)$$

The amplitudes satisfy a set of two coupled Ginzburg-Landau equations that can be derived from the equation for ψ (for instance the Swift-Hohenberg model [22]) by multi scale analysis [9,7],

$$\frac{\partial A}{\partial t} = -\frac{\delta F}{\delta \bar{A}}, \quad \frac{\partial B}{\partial t} = -\frac{\delta F}{\delta \bar{B}}, \quad (2.2)$$

where $\delta F/\delta \bar{A}$ is the functional derivative with respect to the complex conjugate of *A*, and *F* is a Lyapunov functional,

$$F = \int d\vec{r} \mathcal{F} = \int d\vec{r} \left\{ -\epsilon(|A|^2 + |B|^2) + \frac{g}{2}(|A|^4 + |B|^4) + g_\perp |A|^2 |B|^2 + \xi_0^2 \left(\partial_x - \frac{i}{2q_0} \partial_y^2 \right) |A|^2 + \xi_0^2 \left(\partial_y - \frac{i}{2q_0} \partial_x^2 \right) |B|^2 \right\}. \quad (2.3)$$

The coherence length ξ_0 is of the order of q_0^{-1} , *g* and g_\perp are interaction coefficients, and the time scale factor has been set to unity. These three parameters depend on the particular model equation considered for the original field ψ .

The nontrivial stationary solutions $\{A_0, B_0\}$ of the governing set of equations (2.2)-(2.3) describe a planar boundary, and depend only on the coordinate *x* normal to the boundary. They are defined by,

$$0 = \epsilon A_0 + \xi_0^2 \partial_x^2 A_0 - g A_0^3 - g_\perp B_0^2 A_0 \quad (2.4)$$

$$0 = \epsilon B_0 - \frac{\xi_0^2}{4q_0^2} \partial_x^4 B_0 - g B_0^3 - g_\perp A_0^2 B_0. \quad (2.5)$$

This system of equations was extensively studied in refs. [9,10]. It is a planar grain boundary of thickness proportional to $\xi_0/\sqrt{\epsilon}$. Note that the system of equations is not invariant under permutation of A_0 and B_0 . The amplitude A_0 of the rolls parallel to the interface vanishes as $\exp(x\sqrt{\epsilon}/\xi_0)$ when $x \rightarrow -\infty$, and saturates to $(\epsilon/g)^{1/2}\tanh(x\sqrt{\epsilon}/\xi_0)$ when $x \rightarrow +\infty$. The behavior of the amplitude of the rolls perpendicular to the interface is slightly different: $B_0(x) - (\epsilon/g)^{1/2} \propto \exp(x\sqrt{\epsilon}/\xi_0)$ when $x \rightarrow -\infty$, and there is a point x^* such that $B_0(x^*) = 0$. It is customary to define the location of the grain boundary by the point x^* . To a good approximation, $B_0(x) \simeq 0$ for $x \geq x^*$.

We emphasize that a stationary solution only exists when the wavenumber of the solution equals the marginal wavenumber q_0 , and that at first order in ϵ , the solutions A_0 and B_0 only depend on the slow spatial variable $\epsilon^{1/2}x$, but not on the fast scale x . Hence, the location of the boundary and the phase of the rolls are independent [7].

III. LINEAR STABILITY ANALYSIS OF A 90° GRAIN BOUNDARY

We linearize Eqs. (2.2) around $\{A_0, B_0\}$, and assume the following perturbed solutions (note that the form of the perturbation explicitly assumes that the boundary does not undergo a net average displacement),

$$A(x, y, t) = (A_0(x) + \tilde{a})e^{i\tilde{\phi}}, \quad (3.1)$$

$$B(x, y, t) = B_0(x) + \tilde{b}. \quad (3.2)$$

The phase $\tilde{\phi}$ represents a transverse distortion, as shown in Fig. 1b, and is of the general form

$$\tilde{\phi} = \phi(x) \cos(qy)e^{\sigma t}, \quad \tilde{\phi} \ll 1. \quad (3.3)$$

The real fields \tilde{a} and \tilde{b} are amplitude corrections and similarly read,

$$\tilde{a} = a(x) \cos(qy)e^{\sigma t} \quad (3.4)$$

$$\tilde{b} = b(x) \cos(qy)e^{\sigma t}. \quad (3.5)$$

In the above expansion, we have neglected the imaginary part of B . $\mathcal{I}m(B)$ can be written as $d(x) \sin(qy)e^{\sigma t}$; yet, because of the fourth order x -derivative in the equation satisfied by B (the second relation in Eq. (2.2)), $d(x)$ is of order ϵ lower than the real part function $b(x)$, and hence negligible. Inserting Eqs. (3.1)-(3.2) into Eqs. (2.2), we find,

$$\sigma a = \epsilon a + \xi_0^2 [\partial_x^2 a - (q^4/4q_0^2)a - (q^2/q_0)\partial_x(\phi A_0)] - (3gA_0^2 + g_\perp B_0^2)a - 2g_\perp A_0 B_0 b \quad (3.6)$$

$$\sigma A_0 \phi = \xi_0^2 [A_0^{-1} \partial_x (A_0^2 \partial_x \phi) - (q^4/4q_0^2)A_0 \phi + (q^2/q_0)\partial_x a] \quad (3.7)$$

$$\sigma b = \epsilon b - \xi_0^2 q^2 b - (3gB_0^2 + g_\perp A_0^2)b - 2g_\perp B_0 A_0 a. \quad (3.8)$$

We further expand the solutions in power series of the small parameter q^2 , and define, $a = a_0 + q^2 a_2 + q^4 a_4 + \dots$; $\phi = \phi_0 + q^2 \phi_2 + q^4 \phi_4 + \dots$; $b = b_0 + q^2 b_2 + q^4 b_4 + \dots$. Since the limit $q \rightarrow 0$ corresponds to a uniform translation of the interface, $\sigma = q^2 \sigma_2 + q^4 \sigma_4 + \dots$. We now analyze the resulting equations order by order in q^2 .

At order q^0 , Eq. (3.7) reduces to $A_0^2 \partial_x \phi_0 = \text{cst}$. Since $A_0(x)^{-2}$ diverges exponentially at $-\infty$ and $\partial_x \phi$ must remain finite on the whole interval $[-\infty, \infty]$, the only admissible solution is $\partial_x \phi_0 = 0$. Hence $\phi_0 = \text{cst}$ is a free parameter that represents the magnitude of the initial phase modulation. With the notation of Fig. 1b, ϕ_0 is simply related to the magnitude of the roll deformation δx_0 through $\phi_0 = q_0 \delta x_0$ ($\delta x_0 \ll \lambda_0$). At order q^0 , Eqs.(3.6) and (3.8) can be written as

$$H_0 \begin{pmatrix} a_0 \\ b_0 \end{pmatrix} = 0.$$

If we take the x -derivative of Eqs. (2.4) and (2.5) we recover the above equation, with a_0 and b_0 replaced by $\partial_x A_0$ and $\partial_x B_0$. Hence the solutions at this order are:

$$a_0(x) = \alpha_0 \partial_x A_0, \quad b_0(x) = \alpha_0 \partial_x B_0, \quad (3.9)$$

where α_0 is a constant to be determined from the solvability condition at the next order.

At order q^2 , the solutions a_2 and b_2 satisfy,

$$H_0 \begin{pmatrix} a_2 \\ b_2 \end{pmatrix} = \begin{pmatrix} (\alpha_0 \sigma_2 + \phi_0 \xi_0^2 / q_0) \partial_x A_0 \\ \alpha_0 (\sigma_2 + \xi_0^2) \partial_x B_0 \end{pmatrix}. \quad (3.10)$$

The solvability condition at order q^2 requires that the right hand side vector be orthogonal to the kernel of the adjoint of H_0 . Since H_0 is hermitian, and $H_0(\partial_x A_0, \partial_x B_0) = 0$, we find,

$$(\alpha_0 \sigma_2 + \phi_0 \xi_0^2 / q_0) \int_{-\infty}^{\infty} (\partial_x A_0)^2 dx + \alpha_0 (\sigma_2 + \xi_0^2) \int_{-\infty}^{\infty} (\partial_x B_0)^2 dx = 0. \quad (3.11)$$

On the other hand, at order q^2 one can replace $\sigma\phi$ by $\sigma_2\phi_0$, and a by $\alpha_0\partial_x A_0$ in Eq. (3.7). After multiplying Eq. (3.7) by A_0 , and integrating over x , one finds

$$A_0^2 \partial_x \phi_2 = \frac{\sigma_2 \phi_0}{\xi_0^2} \int_{-\infty}^x A_0^2(u) du - \frac{\alpha_0}{q_0} \left[A_0(x) \partial_x A_0(x) - \int_{-\infty}^x (\partial_u A_0)^2 du \right] + C, \quad (3.12)$$

where C is a constant of integration. However, the condition that $|\partial_x \phi_2| < \infty$ when $x \rightarrow -\infty$ requires $C = 0$. Furthermore, in the limit $x \rightarrow +\infty$, $A_0 \rightarrow (\epsilon/g)^{1/2}$, hence $\int^x A_0^2(u) du \propto x$. The gradient of ϕ_2 remains finite only if $\sigma_2 = 0$. Therefore Eq. (3.11) with $\sigma_2 = 0$ now yields the value of the solvability constant α_0 ,

$$\alpha_0 = -\delta x_0 \left(\int_{-\infty}^{\infty} (\partial_x A_0)^2 dx \right) \left(\int_{-\infty}^{\infty} (\partial_x B_0)^2 dx \right)^{-1}, \quad (3.13)$$

where the definition $\phi_0 = q_0 \delta x_0$ has also been used.

To summarize our results up to this point, the perturbed amplitudes at order q^0 are given by,

$$A = [A_0(x) + \alpha_0 \cos(qy) e^{\sigma t} \partial_x A_0(x)] e^{i\tilde{\phi}} \simeq A_0(x + \alpha_0 \cos(qy) e^{\sigma t}) e^{iq_0 \delta x_0 \cos(qy) e^{\sigma t}}, \quad (3.14)$$

$$B \simeq B_0(x + \alpha_0 \cos(qy) e^{\sigma t}), \quad (3.15)$$

where we have used Eqs. (3.1)-(3.2) and (3.9). Equations (3.14) and (3.15) show that the amplitude moduli $|A|$ and $|B|$ of the weakly modulated rolls at this order equal the unmodulated profiles with a simple change in the coordinate origin. By analogy with the planar case [9,10], we define the location of the modulated boundary by the set of points $\{x_g, y\}$ such that $B(x_g, y) = 0$. Eq. (3.15) indicates that the location of the boundary is given by the curve

$$x_g(y) = x^* - \alpha_0 \cos(qy) e^{\sigma t},$$

with $B_0(x^*) = 0$. It is a local translation relative to the planar boundary by $-\alpha_0 \cos(qy) e^{\sigma t}$ along the x -axis. Note, on the other hand, that the lines of constant phase of A are given by $x = cst - \delta x_0 \cos(qy) e^{\sigma t}$ instead, so that $-\delta x_0 \cos(qy) e^{\sigma t}$ represents the local deformation of the straight rolls. As shown by Eq. (3.13), boundary and roll deformations are not independent: the lengths α_0 and δx_0 are related to each other through the non-uniform profiles A_0 and B_0 . A quite non-intuitive result is the opposite directions of the related translations, evidenced by the minus sign in Eq. (3.13). Consider for instance a point where the lines of constant phase of A are displaced towards the region B ; the actual position of the boundary, however, is displaced towards region A . This effect can be seen more easily on Figure 2 (see also Section IV).

At order q^4 integration of Eq. (3.7) leads to,

$$A_0^2 \partial_x \phi_4 = \int_{-\infty}^x \left(\frac{\sigma_4}{\xi_0^2} + \frac{1}{4q_0^2} \right) \phi_0 A_0^2(u) du - \frac{1}{q_0} \int_{-\infty}^x A_0(u) \partial_u a_2 du,$$

where the second order result $\sigma_2 = 0$ has been used. The second integral in the right hand side is finite, but the first one diverges as x when $x \rightarrow +\infty$, except if $\sigma_4/\xi_0^2 + 1/4q_0^2 = 0$. We therefore conclude that, at leading order in q

$$\sigma = -\frac{\xi_0^2}{4q_0^2} q^4. \quad (3.16)$$

This is one of the central results of this section: the modulated boundary is expected to relax exponentially with a rate proportional to q^4 .

The linear analysis shows that the interface is always stable with respect to long wavelength perturbations. This is in agreement with the case studied in ref. [21], although the authors concluded that the decay rate $\sigma \propto q^2$ instead. Such a behavior was found because the wave vector of the modulation considered in their work had a nonzero component in the longitudinal direction. We note that the decay rate of Eq. (3.16) is in fact identical to that of a single wave (A -rolls only in Figure 1) [7]. According to Eq. (3.16), the relaxation of the boundary is completely determined by the relaxation of the A rolls far from it.

Unfortunately, in spite of the fact that the main predictions of the perturbation analysis agree well with a numerical solution of the Swift-Hohenberg equation, the linear analysis just discussed is not uniformly valid (we will further elaborate on this point in Section V). Consider Eq. (3.12) for ϕ_2 in the limit $x \rightarrow +\infty$. The leading behavior is given by

$$\phi_2 \simeq \frac{\alpha_0}{q_0 A_0^2(\infty)} \left(\int_{-\infty}^{\infty} (\partial_u A_0)^2 du \right) x. \quad (3.17)$$

Therefore the phase perturbation $\phi \simeq \phi_0 + q^2 \phi_2$, which is assumed to be small in the derivation of Eq. (3.7), diverges as x for large x through the second order correction ϕ_2 at any finite time t . As a consequence, from Eq. (3.3), the y -component of the wavevector of the roll pattern is,

$$\partial_y \tilde{\phi} = -q \sin(qy) e^{\sigma t} (\phi_0 + q^2 \phi_2),$$

and also diverges with x . This implies that, far enough from the boundary, the y -component of the wave vector becomes larger than the x component, given by $q_0 + \partial_x \tilde{\phi} \simeq q_0$. This solution represents an increasingly zig-zagging wave, which is of course not physical. As it is apparent from Eq. (3.17), the singularity arises because of the presence of a non-uniform amplitude of the pattern near the boundary $\partial_x A_0 \neq 0$. In fact, we think it is possible that the linearized system with non-constant coefficients (3.6)-(3.8) does not have bounded eigenfunctions.

It appears that the failure of the linear analysis is related to an additional important feature of boundary motion, not taken into account in the previous calculation: a net translation of the average position of the boundary towards the A -region, as shown by the numerical calculations presented in the following Section. After we present the numerical evidence, we argue in Section V that this feature cannot be obtained at the linear level in the amplitude of the perturbation, and that it is in fact a singular contribution in the limit $\epsilon \rightarrow 0$.

IV. NUMERICAL SOLUTION OF THE SWIFT-HOHENBERG EQUATION

In order to test the predictions of the previous Section, and to obtain further insight into grain boundary motion, we have numerically solved the Swift-Hohenberg model of Rayleigh-Bénard convection, [22]

$$\frac{\partial \psi}{\partial t} = \epsilon \psi - \frac{\xi_0^2}{4q_0^2} (q_0^2 + \nabla^2)^2 \psi - \psi^3. \quad (4.1)$$

We consider the evolution from an initial condition that corresponds to the geometry shown in Fig. 1b. We note that solving Eq. (4.1) in the case of curved rolls is much simpler than solving the two dimensional Ginzburg-Landau equations (2.2).

Equation (4.1) is solved numerically with a pseudo-spectral method. Further details on the algorithm and the time integration scheme can be found in ref. [23]. The stability of the algorithm allows relatively large values of the time step, which is fixed to 0.4 in the dimensionless time units of Eq. (4.1). Equation (4.1) is then discretized on a square grid of size 512×512 , and occasionally 256×256 . Spatial discretization is such that there are 8 grid nodes per wavelength λ_0 . In all the following numerical examples, we have chosen $\xi_0 = 2q_0^{-1}$, which is close to the value that corresponds to the stress free boundary conditions in the original system of fluid mechanical equations, from which the Swift-Hohenberg equation is derived as an approximation. We use periodic boundary conditions in both directions, and hence the initial condition comprises two symmetric, well separated grain boundaries located at $x = 1/4$ and $x = 3/4$, in units of the system size. We have verified that the numerical solutions of the Swift-Hohenberg equation for the stationary straight grain boundary coincides with those obtained by directly solving the amplitude equations (2.4)-(2.5), with the appropriate parameters that follow from the multi-scale analysis of the Swift-Hohenberg equation ($g = 3/4$ and $g_{\perp} = 3/2$). The modulated initial condition is implemented with the help of the one dimensional solution, as

$$\psi(x, y, t = 0) = A_0(x) \cos[q_0 x + q_0 \delta x_0 \cos(qy)] + B_0(x) \cos[q_0 y]. \quad (4.2)$$

A typical configuration is shown in Figure 2, taken at the intermediate time $t = 1600$, with $\epsilon = 0.04$, $q = q_0/16$ and a system size of 256×256 . Note that this solution is consistent with our earlier assumption of neglecting $\mathcal{I}m(B)$ in the perturbation equations (Eq. (3.2)), since the B rolls remain straight near the grain boundary despite of the transverse modulation of the A rolls. The opposition in phase of the roll profile and of the boundary location, given

in Eq. (3.13), is also well reproduced numerically. Yet, this effect is easy to observe only for relatively large values of δx_0 , as shown on Fig. 2.

Figure 3 shows our numerical results for the inverse decay rate $-\sigma^{-1}$ as a function of q . These results are obtained for a system of size 512×512 , so that the number of rolls that separate the two grain boundaries is twice larger than in Figure 2. We checked that the planar grain boundaries did not appreciably interact, and therefore remained stationary. The value of σ was determined from an exponential fit to the decay of the phase of a given roll, for a small initial δx_0 . We first compute numerically σ in the absence of any grain boundary, *i.e.* with the single wave A . We find very good agreement with Eq. (3.16), given that there are no adjustable parameters in the theoretical curve. When grain boundaries are present, the numerical results (square symbols) are somewhat higher, but still compare well with Eq. (3.16). They remain closer to the law $\sigma \propto -q^4$, rather than to, say, $\sigma \propto -q^5$, and certainly than to $\sigma \propto -q^2$. The small discrepancy observed is probably due to the finite size of the system: although the two grain boundaries are separated by roughly 30 rolls, they slightly interact during relaxation. As a check, we have computed $\sigma(q = 3q_0/32)$ again in a system of size 1024×1024 , with same value of λ_0 . The difference between that numerical result and the theoretical curve is reduced by a factor of 2.5 compared with a system size of 512×512 .

The numerical solution reveals an additional feature which was not included in our linear analysis: while the boundary modulation is relaxing, there is net motion of the grain boundary towards the A roll region. This motion is a pure amplitude mode, as the lines of constant roll phase remain stationary on average. Therefore, after a long time, the modulated rolls have completely relaxed but the size of the region of A rolls has decreased, and the grain boundary is located at a distance d_∞ away from its initial average location. The distance d_∞ exceeds the initial deformation δx_0 , and it can be even significantly larger than the roll wavelength λ_0 . In the configuration shown in Fig. 2 (system of size 256×256), the magnitude of the perturbation was deliberately chosen relatively large ($\delta x_0 = \lambda_0$), so that, at late times, the modulated region completely disappears by annihilation of the two grain boundaries.

We now report our results for d_∞ in a bigger system of size 512×512 , and with $q = 3q_0/32$. Figure 4 shows our results for the total traveled distance d_∞ as a function of δx_0 . The complete relaxation of the perturbation requires times around 10^5 , and the location of the (nearly) flat boundary is again defined to be the point x^* at which $B(x^*) = 0$ [9]. This point is obtained from the field ψ through the relation $B(x) = [\psi(x, y = \lambda_0) - \psi(x, y = 3\lambda_0/2)]/2$ for a flat interface (see Eq. (2.1)). We observe in the figure that the total traveled distance increases nonlinearly with δx_0 . The following Section gives an interpretation of this feature, and further discussion of the results.

V. DEFECT MOTION THROUGH ENERGY RELAXATION

We study in this section a more general form for the perturbed amplitudes than those given in Eqs. (3.14)-(3.15). We assume a perturbed solution of the form,

$$A = A_0(x - \kappa\delta x(t) \cos(qy) - d(t)) e^{iq_0\delta x(t) \cos(qy)} \quad (5.1)$$

$$B = B_0(x - \kappa\delta x(t) \cos(qy) - d(t)) \quad (5.2)$$

where

$$\delta x(t) = \delta x_0 e^{\sigma t}, \quad \sigma = -\frac{\xi_0^2}{4q_0^2} q^4, \quad \text{and } \kappa = \int (\partial_x A_0)^2 dx / \int (\partial_x B_0)^2 dx. \quad (5.3)$$

The quantity $d(t)$ represents the net distance traveled by the grain boundary at time t . A linear stability analysis based on (5.1)-(5.2) along the lines of Section III leads to $d(t) = 0$ for an interface initially located at the origin. As we show below, the net displacement depends nonlinearly on the initial modulation, and hence cannot be obtained from a linearized set of equations. We use here a different method that has been widely used to study of defect motion in potential systems [1]. It is based on the identity,

$$\frac{dF}{dt} = -2 \int d\vec{r} \left(\left| \frac{\partial A}{\partial t} \right|^2 + \left| \frac{\partial B}{\partial t} \right|^2 \right), \quad (5.4)$$

directly derived from Eqs. (2.2)-(2.3).

The left hand side of Eq. (5.4) can be calculated approximately by substituting Eqs. (5.1) and (5.2) into Eq. (2.3), and taking the time derivative. After some algebra, we find,

$$\frac{dF}{dt} = \int d\vec{r} \left\{ -\dot{d} \partial_x \mathcal{F}_0 + \frac{\xi_0^2 q^4}{4} \cos^2(qy) \left[2\delta x \dot{\delta x} A_0^2(u) - \delta x^2 \dot{d} \partial_x A_0^2(u) \right] \right\}, \quad (5.5)$$

up to order δx^2 . \mathcal{F}_0 is the free energy density of a planar boundary, and $u = x - \kappa \delta x(t) \cos(qy) - d(t)$. The term involving \mathcal{F}_0 vanishes since $\mathcal{F}_0(x = +\infty) = \mathcal{F}_0(x = -\infty)$. In Eq. (5.5), we have neglected the contributions from the terms $\partial_y A_0(u)$ and $\partial_y B_0(u)$; they are of order $\epsilon^{1/2}$ smaller than $A_0(u) \partial_y e^{i\phi}$ because of the slow variations of the amplitudes compared with the roll periodicity. In addition, we have used the approximation $\partial_t A_0(u) \simeq -\dot{d} \partial_x A_0(u)$ by neglecting $-\kappa \dot{\delta x}(t) \cos(qy) \partial_x A_0(u)$: the contributions proportional to this last term vanish with $\int \cos(qy) dy$ at leading order in ϵ when spatial integration over y is performed in Eq. (5.5). For the same reason, all terms proportional to δx in Eq. (5.5) do not contribute.

By using similar considerations, the right hand side of Eq. (5.4) at leading order in ϵ and $\delta x(t)$ reads,

$$-2 \int d\vec{r} \left\{ \dot{d}^2 [(\partial_x A_0(u))^2 + (\partial_x B_0(u))^2] + (\delta \dot{x})^2 q_0^2 \cos^2(qy) A_0^2(u) \right\}. \quad (5.6)$$

By combining Eqs. (5.5) and (5.6), and by using Eq. (5.3) for $\delta x(t)$, we find that all terms that do not involve \dot{d} cancel, and obtain

$$\dot{d}(t) = \left(\frac{\xi_0^2}{4q_0^2} q^4 \right) \frac{\epsilon}{4g} \frac{[q_0 \delta x(t)]^2}{\int_{-\infty}^{\infty} dx [(\partial_x A_0)^2 + (\partial_x B_0)^2]}, \quad (5.7)$$

where we have used the identities $A_0^2(+\infty) = \epsilon/g$ and $\int_0^L dy \cos^2(qy)/L = 1/2$, where L is the length of the grain boundary. Equation (5.7) shows that $\dot{d} > 0$; i.e., in the configuration shown in Fig. 1 the motion of the boundary is such that the modulated rolls are progressively replaced by the advancing perpendicular straight rolls. Furthermore, and contrary to the usual motion of kinks, the velocity is not constant but decreases as $\delta x(t)^2$. Since at long times $\delta x(t) \simeq 0$, the boundary eventually stops. In Appendix A, we show that Eq. (5.7) generalizes the equation describing the uniform motion of a grain boundary through a time independent modulated background. The method presented in Appendix A also provides a simpler alternative way to extend the result (5.7) to the case in which the transversally modulated rolls are not parallel to the grain boundary.

Equations (5.3) and (5.7) can now be used to calculate the total distance traveled by the grain boundary d_∞ , allowing further comparison with the numerical results of Section IV. We find,

$$d_\infty = \frac{\epsilon}{8g} \frac{(q_0 \delta x_0)^2}{\int_{-\infty}^{\infty} dx [(\partial_x A_0)^2 + (\partial_x B_0)^2]}. \quad (5.8)$$

Note that, in contrast to \dot{d} , d_∞ does not depend on the wavenumber of the modulation q , for small q . Since $A_0(x) = \sqrt{\epsilon/g} f(\sqrt{\epsilon} x/\xi_0)$ at leading order in ϵ , and if a similar form is assumed for B_0 , it is easy to see from Eqs. (5.7) and (5.8) that \dot{d} and d_∞ are proportional to $\epsilon^{-1/2}$ [24]. Hence the displacement of the boundary diverges close to onset, regardless of the initial amplitude of the modulation. Eqs. (5.7) and (5.8) also show that the magnitude of this displacement depends quadratically on the perturbation δx_0 , explaining why it can not be derived from the linear analysis presented in Section III. Finally, we note that the velocity $\dot{d}(t)$ is proportional to $\epsilon^{-1/2} \delta x(t)^2 q^4$, at leading order in ϵ , $\delta x(t)$ and q .

The mechanism for net grain boundary motion can be understood as the follows: Relaxation requires energy decrease while straight rolls have the same energy regardless of their orientation (both base states A and B, are in principle degenerate). However, when the boundary is modulated in the way depicted in Fig. 2, only the rolls parallel to the boundary are distorted at lowest order in ϵ , whereas the perpendicular rolls remain straight. Therefore, the energy of the modulated configuration can decrease by both linear relaxation of the initially curved rolls and by nonlinear net displacement of the grain boundary, the effect of which is to replace curved rolls by straight ones. Close to onset, relaxation through the nonlinear mode is dominant, and even a small perturbation δx_0 can induce a large boundary displacement $d_\infty \gg \delta x_0$. Of course, for fixed ϵ , d_∞ goes to zero with δx_0 . It is precisely the observation that the amplitude of this nonlinear mode diverges at $\epsilon \rightarrow 0$ that suggests that the linearized problem discussed in Section III may not have any bounded eigenfunctions.

At fixed ϵ , it is instructive to obtain the magnitude of δx_0 above which the velocity of the boundary is much larger than the phase velocity of the rolls; i.e.,

$$\dot{d}(t=0) \gg |\delta \dot{x}(t=0)|. \quad (5.9)$$

In this limit, boundary motion occurs at approximately constant roll phase. Given that $\delta \dot{x}(0) = \sigma \delta x_0$, and by using Eq. (5.7) for $\dot{d}(0)$, Eq. (5.9) leads to

$$\delta x_0 \gg \left(\frac{\lambda_0}{2\pi} \right)^2 \frac{4g}{\epsilon} \int_{-\infty}^{\infty} dx [(\partial_x A_0)^2 + (\partial_x B_0)^2].$$

With the numerical solutions obtained for $A_0(x)$ and $B_0(x)$ from the coupled Ginzburg-Landau equations, we find that $\delta x_0 \gg 5.0 \cdot 10^{-2} \lambda_0$ for $\epsilon = 0.04$, and $\delta x_0 \gg 7.4 \cdot 10^{-2} \lambda_0$ for $\epsilon = 0.1$. Therefore we conclude that nonlinear motion dominates linear relaxation even for relatively small initial perturbations. We recall that our perturbative calculation is valid if $\delta x_0 < \lambda_0$.

We have verified that d_∞ does not appreciably depend on the wavelength of the modulation, as shown in Eq. (5.8). Figure 4 shows our analytical and numerical results of the total distance traveled by the grain boundary as a function of δx_0 . The theoretical curve has no adjustable parameters, and is based on the numerical resolution of Eqs. (2.4)-(2.5) with the values $g = 3/4$ and $g_\perp = 3/2$ that correspond to the Swift-Hohenberg equation. We performed two series of runs, for $\epsilon = 0.04$ and $\epsilon = 0.1$. At $\epsilon = 0.04$, Eq. (5.8) is in quantitative agreement with the numerical data for small modulations. The discrepancy observed at large modulation indicates the breakdown of the linear relaxation of $\delta x(t)$: perturbations start decaying at a faster rate than (3.16), so that Eq. (5.8) is over-estimating the traveled distance at short times. At $\epsilon = 0.1$, we expect a smaller displacement d_∞ , for fixed δx_0 , than in the case $\epsilon = 0.04$. This is what we observe. However, the numerical results show that d_∞ does not vary continuously with δx_0 , but rather it increases discontinuously. As it is apparent in Figure 4 (crosses), d_∞ takes now only multiple values of half the wavelength of the pattern. A lower threshold is needed to displace the grain boundary, which we estimate to be $\delta x_c \simeq \lambda_0/7$. These observations cannot be explained by the present analysis, and reveal non-adiabatic effects that go beyond the amplitude equation formalism. Such effects have been previously observed in other studies of fronts propagation [1,25]. The underlying cause is that with increasing ϵ the variations of A in the slow variable $\epsilon^{1/2}x$ do not decouple with the fast variable describing the underlying periodic structure. In this case, the solution for the amplitudes depends on the position of the rolls.

VI. CONCLUSIONS

We have found an additional mechanism for grain boundary motion in layered phases which is driven by roll curvature in the vicinity of the boundary. We have analytically studied the motion of an isolated grain boundary within the amplitude equations formalism, and numerically by direct solution of the Swift-Hohenberg equation. Transverse perturbations of the rolls near the grain boundary decay exponentially in time with a rate proportional to q^4 , where q is the wavenumber of the perturbation. In addition, we have found a nonlinear mode involving net translation of the average location of the boundary. On the basis of functional minimization, this mode is preferred to simple linear relaxation near onset. The net velocity of the grain boundary has been computed, and is given in Eq. (5.7). This result can be interpreted as giving the velocity as the ratio between a time dependent external force imposed by curved rolls, and a drag term or mobility that depends on the local amplitude profile of the grain boundary. Close to onset, the drag term goes to zero as $\epsilon^{3/2}$, and makes the interface velocity (and the total traveled distance) diverge as $\epsilon^{-1/2}$. We have argued that this motion cannot be explained by linear analysis.

The precise relationship between these results and the related problem of coarsening of layered phases requires further study. However, we can offer a few comments based on the results presented in this paper. If the temporal evolution of a disordered configuration were controlled by the relaxation of an ensemble of grain boundaries moving through a background of curved rolls, then Eq. (5.7) could be used to infer the coarsening rate. If v is a characteristic grain boundary speed, and κ is the characteristic curvature of the rolls ahead of the boundary, then Eq. (5.7) leads to $v \propto \kappa^2$. If self-similarity holds during the coarsening of the structure, this last relationship would imply a coarsening law $l(t) \sim t^{1/3}$, where $l(t)$ is any measure of the linear scale of the structure. This result for the coarsening law disagrees with previous literature on the subject [17,12,5,18–20].

Although the configuration studied in this paper is idealized, it is conceivable that it describes one among possibly many competing mechanisms during coarsening. A numerical solution of the two dimensional Swift-Hohenberg equation close to onset shows that curved rolls are essentially immobile due to topological constraints (mostly disclinations), whereas grain boundaries move over large distances. It is likely that the motion of the latter is in part due to a background of curved rolls with a characteristic curvature which is set by the spatial distribution of disclinations. Disclinations, in turn, can be eliminated by grain boundary motion. If the characteristic length scales associated with both defects (grain boundary perimeter and disclination separation) are proportional to each other, as required by self-similarity, then $t^{1/3}$ would be a possible contribution to the coarsening law. Whether this mechanism would dominate the asymptotic behavior as $l \rightarrow \infty$ is being currently investigated.

ACKNOWLEDGMENTS

This research has been supported by the U.S. Department of Energy, contract No. DE-FG05-95ER14566, and also in part by the Supercomputer Computations Research Institute, which is partially funded by the U.S. Department of Energy, contract No. DE-FC05-85ER25000.

APPENDIX A: GRAIN BOUNDARY MOTION WITHOUT PHASE RELAXATION

Equation (5.7) can be derived in an different way, which is similar to the calculation of the velocity of a climbing dislocation [1]. Suppose that a set of rolls is modulated along the transverse direction, with wave vector \vec{q} , and is rigidly held with a time independent modulation amplitude δx_f . Hence, the system is allowed to evolve by rigid translation alone, and no roll (or boundary) relaxation is allowed. We then introduce the perturbations (5.1)-(5.2) with $\delta x(t) = \delta x_f$. Equation (5.4) can be simply recast as

$$\dot{d} \int dy \{ \mathcal{F}(x = -\infty, y) - \mathcal{F}(x = +\infty, y) \} = -2\dot{d}^2 \int d\vec{r} [|\partial_x A|^2 + |\partial_x B|^2] , \quad (\text{A1})$$

where \dot{d} is the constant velocity of the grain boundary. The left-hand side of Eq. (A1) represents the free energy lost per unit time by the system as the grain boundary moves. The straight rolls, of lower free energy, replace curved ones. The difference dF is computed that corresponds to increasing the area of the domain occupied by B straight rolls by an amount $\dot{d} dt$, and by decreasing by the same amount the area of the domain occupied by A curved rolls. The free energy gain is easily computed by using Eq. (2.3) with $B(-\infty) = (\epsilon/g)^{1/2}$, $A(-\infty) = 0$, and $B(+\infty) = 0$, $A(+\infty) = (\epsilon/g)^{1/2} e^{iq_0 \delta x_f \cos(qy)}$. In the right-hand side of Eq. (A1), $|\partial_x A(B)|$ is replaced by $|\partial_x A_0(B_0)|$ at leading order. Eq. (A1) yields Eq. (5.7) straightforwardly, where $\delta x(t)$ must be replaced by δx_f . By using Eq. (A1), the numerator of Eq. (5.7) can now be interpreted as a (time dependent) external force acting on the line defect, the denominator being the drag term or friction coefficient. It is interesting to note that the more rigorous analysis of the combined effects of roll relaxation and front advance that leads to Eq. (5.7) gives the same expression as when roll relaxation is omitted. Beside being simpler, an additional advantage of the energy argument presented here is that it can be applied to a configuration where the set of rolls A and B are not parallel nor perpendicular to the grain boundary. In this case, the external force $\int dy \{ \mathcal{F}(x = -\infty, y) - \mathcal{F}(x = +\infty, y) \}$ remains unchanged, by rotational invariance. Only the drag term would probably differ, because of the different grain boundary profile. However, we expect that the scaling behavior $\dot{d} \propto \delta x^2 q^4$ still holds.

- [1] M. Cross and P. Hohenberg, Rev. Mod. Phys. **65**, 851 (1993).
- [2] M. Seul and D. Andelman, Science **267**, 476 (1995).
- [3] G. Fredrickson and F. Bates, Annu. Rev. Mater. Sci. **26**, 501 (1996).
- [4] M. Cross and A. Newell, Physica D **10**, 299 (1984).
- [5] M. Cross and D. Meiron, Phys. Rev. Lett. **75**, 2152 (1995).
- [6] J. Toner and D. Nelson, Phys. Rev. B **23**, 316 (1981).
- [7] P. Manneville, *Dissipative Structures and Weak Turbulence* (Academic, New York, 1990).
- [8] E. Siggia and A. Zippelius, Phys. Rev. A **24**, 1036 (1981).
- [9] P. Manneville and Y. Pomeau, Phil. Mag. A **48**, 607 (1983).
- [10] G. Tesauro and M. Cross, Phil. Mag. A **56**, 703 (1987).
- [11] H. Brand and K. Kawasaki, J. Phys. A **17**, L905 (1984).
- [12] K. Elder, J. Viñals, and M. Grant, Phys. Rev. A **46**, 7618 (1992).
- [13] A. Bray, Phys. Rev. E **58**, 1508 (1998).
- [14] P. Hohenberg and B. Halperin, Rev. Mod. Phys. **49**, 435 (1977).
- [15] A. Bray, in *Formation and interaction of topological defects*, edited by A.-C. Davis and R. Brandenberger (Plenum, New York, 1995).
- [16] G. Mazenko, in *Formation and interaction of topological defects*, edited by A.-C. Davis and R. Brandenberger (Plenum, New York, 1995).
- [17] K. Elder, J. Viñals, and M. Grant, Phys. Rev. Lett. **68**, 3024 (1992).

- [18] Y. Shiwa, T. Taneike, and Y. Yokojima, Phys. Rev. Lett. **77**, 4378 (1996).
- [19] Q. Hou, S. Sasa, and N. Goldenfeld, Physica A **239**, 219 (1997).
- [20] J. Christensen and A. Bray, Phys. Rev. E **58**, 5364 (1998).
- [21] B. Malomed, A. Nepomnyashchy, and M. Tribelsky, Phys. Rev. A **42**, 7244 (1990).
- [22] J. Swift and P. Hohenberg, Phys. Rev. A **15**, 319 (1977).
- [23] M. Cross, D. Meiron, and Y. Tu, Chaos **4**, 607 (1994).
- [24] Actually, the dependence of $\int dx(\partial_x B_0)^2$ with ϵ differs slightly from $\int dx(\partial_x A_0)^2 \sim \epsilon^{3/2}$ (see ref. [9]). However, the behavior $\dot{d} \propto \epsilon^{-1/2}$ remains a good approximation.
- [25] D. Bensimon, B. Shraiman, and V. Croquette, Phys. Rev. A **38**, 5641 (1988).

FIG. 1. a) Grain boundary separating two set of rolls A and B of same periodicity ($|\vec{q}_0| = |\vec{q}'_0| = q_0$). The rolls of domain A are weakly curved by a transverse modulation of wavenumber $q \ll q_0$. b) Particular case studied here, corresponding to a 90° orientation. δx_0 is the magnitude of the phase modulation.

FIG. 2. Configuration with curved interfaces obtained by numerical solution of the Swift-Hohenberg equation in a square grid with 256×256 nodes, with $\epsilon = 0.04$, $q = q_0/16$ and $\delta x_0 = \lambda_0 = 8$. Because of the curved rolls, the grain boundaries are moving towards each other.

FIG. 3. Decay time $-\sigma^{-1}$ (in dimensionless time units) of the grain boundary modulation as a function of wavenumber q . The square symbols are the numerical results while the solid line corresponds to Eq. (3.16). The cross symbols are the numerical results obtained from the modulation of a single wave, without any grain boundary.

FIG. 4. Total distance traveled by the interface d_∞ as a function of the magnitude of the initial modulation δx_0 , for $\epsilon = 0.04$ and $\epsilon = 0.1$. ($q = 3q_0/32$, the grid size is 512×512 and $\lambda_0 = 8$). The symbols are the numerical results, and the solid line corresponds to Eq. (5.8).

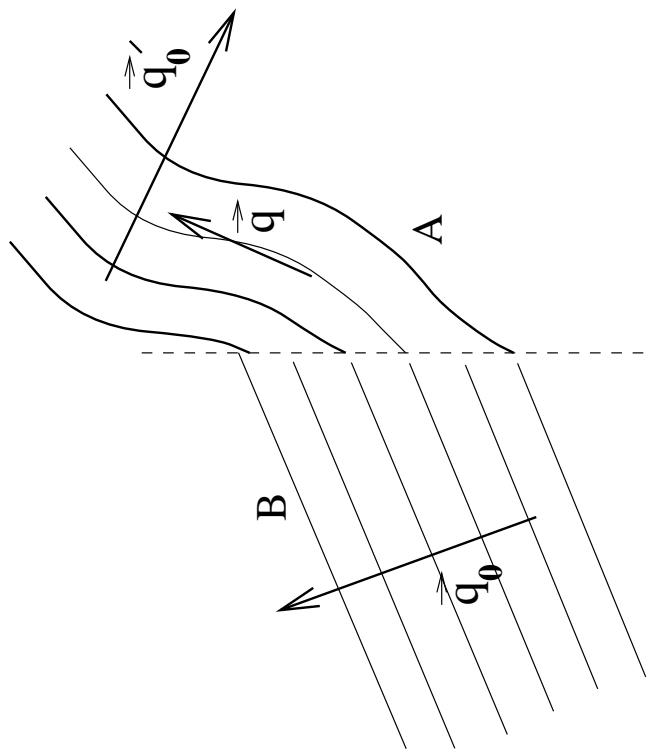


Fig. 1a

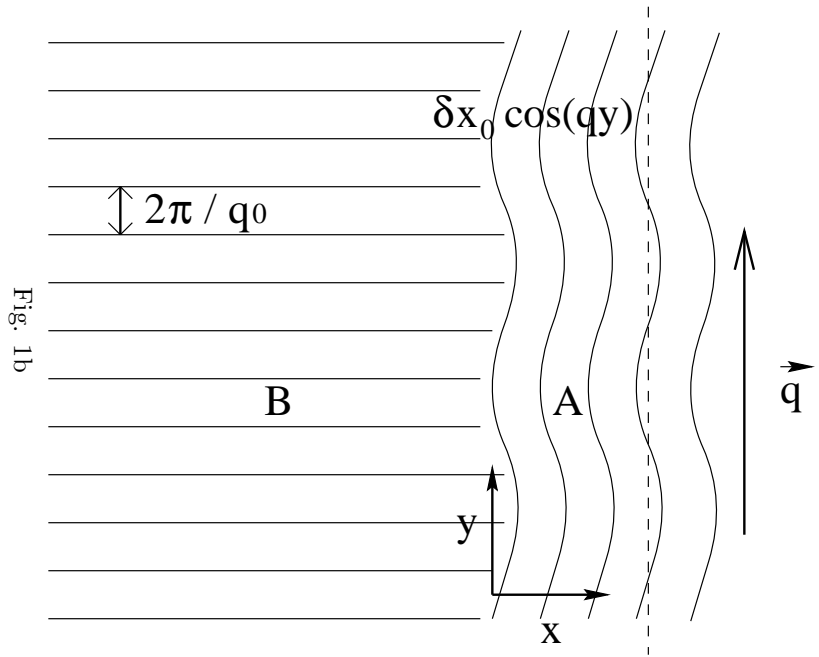


Fig. 1b

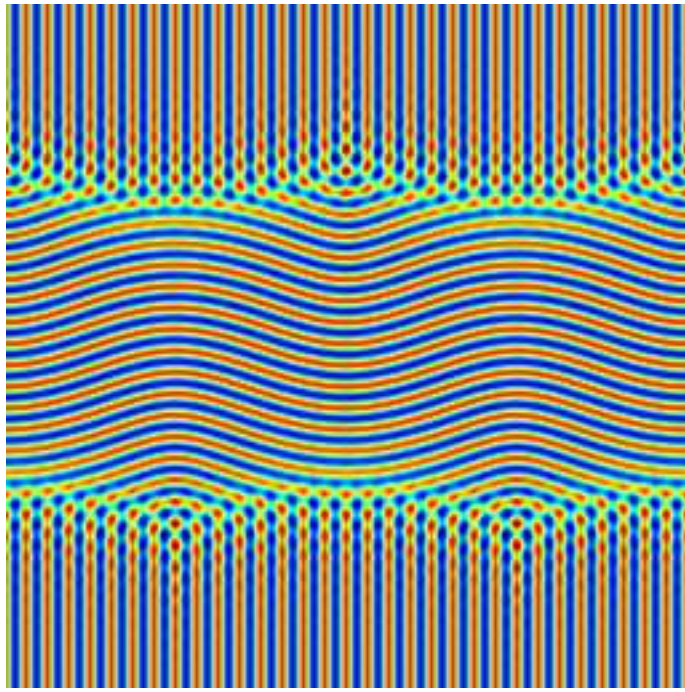


Fig. 2

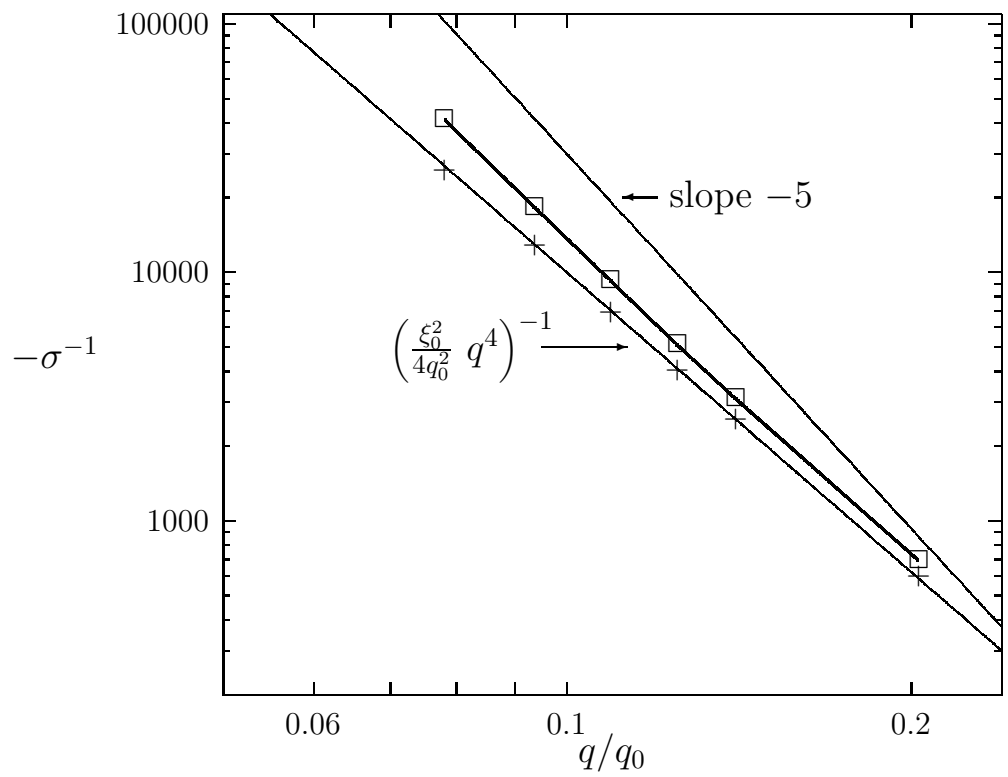


Fig. 3

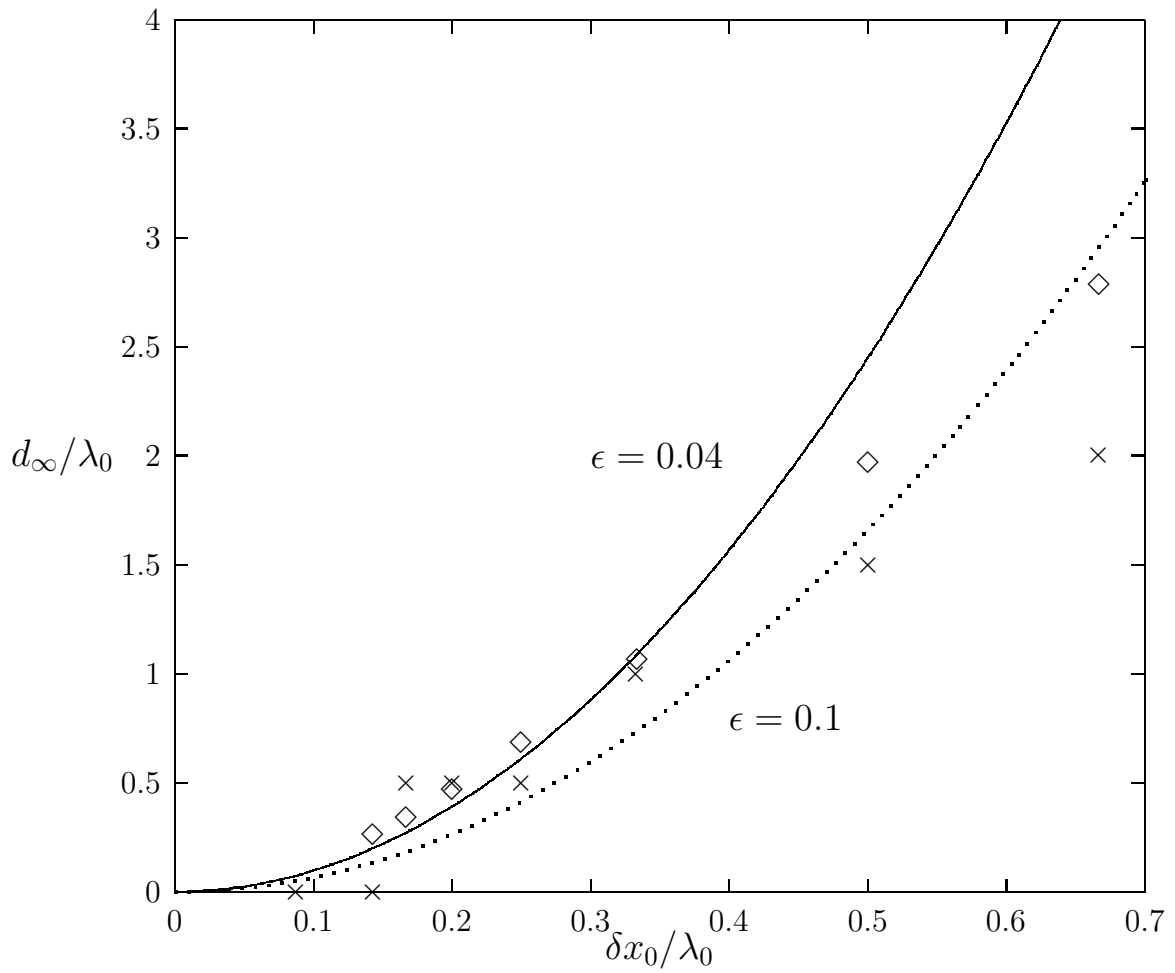


Fig. 4